International Journal of Heat and Mass Transfer 52 (2009) 597–609

Contents lists available at ScienceDirect

International Journal of Heat and Mass Transfer

journal homepage: www.elsevier.com/locate/ijhmt

Numerical simulation of parabolic trough solar collector: Improvement using counter flow concentric circular heat exchangers

O. García-Valladares [a,*], N. Velázquez [b]

[a] Centro de Investigación en Energía, Universidad Nacional Autónoma de México, Privada Xochicalco s/n, Temixco, Morelos 62580, Mexico
[b] Instituto de Ingeniería, Universidad Autónoma de Baja California, Blvd. Benito Juárez y Calle de la Normal s/n, Mexicali, Baja California 21280, Mexico

ARTICLE INFO

Article history:
Received 2 April 2008
Received in revised form 7 August 2008
Available online 20 September 2008

Keywords:
Concentration
PTC
Numerical model
Solar energy
Heat exchanger
Double pipe

ABSTRACT

Detailed numerical simulations of thermal and fluid-dynamic behavior of a single-pass and double-pass solar parabolic trough collector are carried out. The governing equations inside the receiver tube, together with the energy equation in the tube walls and cover wall and the thermal analysis in the solar concentrator were solved iteratively in a segregated manner. The single-pass solar device numerical model has been carefully validated with experimental data obtained by Sandia National Laboratories. The effects of recycle at the ends on the heat transfer are studied numerically shown that the double-pass can enhance the thermal efficiency compared with the single-pass.

1. Introduction

In order to deliver high temperatures with good efficiency a high performance solar collector is required. Systems with light structures and low cost technology for process heat application up to 400 °C could be obtained with Solar Parabolic Trough Collector (solar PTC). These systems can effectively produce temperatures between 50 and 400 °C [1].

PTCs are made by bending a sheet of reflective surface into a parabolic shape. Typically a single phase fluid circulating through a metal black tube receiver, covered with a glass tube (with vacuum or air in the space between the receiver and cover) to decrease convective heat losses, is placed along the focal line of the receiver. The surface of receiver is typically covered with a selective coating that has a high absorptance for solar radiation, but low emittance for thermal radiation loss. It is sufficient to use a single axis tracking of the sun and thus long collector modules that are supported by pedestals are produced.

Solar PTC with evacuated tubular receivers is the main technology currently used in solar thermal electrical power plants (but it is also used in steam generation, absorption cooling, seawater distillation, etc.) because of considerable experience with the systems and the development of small commercial industry to produce and market these systems.

Sandia National Laboratories performed test on a typical solar PTC to determine the thermal loss and collector efficiency of the LS2 Solar Thermal Electric Generation Systems (SEGS) [2]. Chrome black and Cermet selective coatings were studied together with three receiver configurations: glass envelope with vacuum or air in the receiver annulus, and a bare receiver tube. Dudley et al. [2] derived performance correlations relating collector efficiency and thermal loss to working fluid temperature by simple polynomial correlation of the test data. An incidence angle modifier was also developed by measuring the efficiency of the collector for a range of incidence angles.

A direct steam generation collector (DSG) has been proposed [3] as a development of the SEGS in order to eliminate the costly synthetic oil, intermediate heat transport piping loop and oil to stream heat exchanger. Kalogirou et al. [4] analyzed a low pressure steam generation system which is based on heating water in a PTC and then flashing to steam in a separate vessel. The flow in the solar PTC is maintained in the liquid phase region.

A thermal model of a DSG collector was developed by Odeh et al. [5,6] to model heat loss in terms of receiver wall temperature rather than working fluid temperatures. When the model is compared with the Sandia test data, it was found to underestimate the measured loss. Odeh and Morrison [7] developed a transient numerical model for analyzing the performance of industrial water heating systems using PTC.

Nowadays, it is under construction Andasol 1, 2 and 3 in Spain. These are plants of 50 MW based on a series of parabolic troughs, huge curved mirrors about 5.5 m wide. The mirrors slowly track the sun from east to west, and oil reaches about 400 °C.

In this paper, firstly a detailed numerical simulation of optical, thermal and fluid-dynamic behavior of a single-pass solar PTC is

* Corresponding author. Tel.: +52 55 56229746; fax: +52 55 56229791.
E-mail address: ogv@cie.unam.mx (O. García-Valladares).

0017-9310/$ - see front matter © 2008 Elsevier Ltd. All rights reserved.
doi:10.1016/j.ijheatmasstransfer.2008.08.004

Nomenclature

A_{ref}	aperture area ($W \cdot L$) [m^2]
A_t	fluid flow cross-section area [m^2]
$A_{t,c}$	cover tube cross-section area [m^2]
$A_{t,r}$	receiver tube cross-section area [m^2]
C	concentration ratio [dimensionless]
Cp	specific heat at constant pressure [J/(kg K)]
D	diameter [m]
e	specific energy ($H + v^2/2 + gz\sin\theta$) [J/kg]
exp	experimental
fr	friction factor [dimensionless]
F	focal distance [m]
F_a	incident angle modifier [dimensionless]
F_{rc}	view factor between receiver and cover [dimensionless]
g	gravitational constant [m/s^2]
h	heat transfer coefficient [W/(m^2 K)]
H	enthalpy [J/kg]
I	solar irradiance [W/m^2]
I_D	improvement of solar PTC performance defined by Eq. (44) [%]
k	thermal conductivity [W/(m K)]
K	channel thickness ratio ($D_{i,\text{int}}/D_{r,\text{int}}$) [dimensionless]
L	receiver length [m]
m	mass [kg]
$\dot{m}$	mass flow rate [kg/s]
M	recycle ratio [dimensionless]
n	number of control volumes [dimensionless]
Nu	Nusselt number [dimensionless]
p	pressure [bar]
P	perimeter [m]
P_T	friction power expenditure defined by Eq. (45) [W]
Pr	Prandtl number [dimensionless]
$\dot{q}$	heat flow per unit area [W/m^2]
$\dot{q}_u$	useful energy gain per receiver unit area [W/m^2]
$\dot{q}_{wall}$	heat flux from wall to fluid per receiver unit area [W/m^2]
$\dot{Q}$	heat flow [W]
$\dot{Q}_u$	energy gain [W]
Ra	Rayleigh number [dimensionless]
Re	Reynolds number [dimensionless]
S	solar absorbed energy per unit area [W/m^2]
t	time [s]
T	temperature [K]
v	velocity [m/s]
W	collector width [m]
x_g	vapor quality [dimensionless]
z	axial coordinate

Greek symbols

α	absorptance [dimensionless]
δ	rate of convergence [K]
ε	emittance [dimensionless]
ε_g	void fraction [dimensionless]
ϕ	aperture angle [rad]
γ	shape factor due to inexact concentrator orientation [dimensionless]
η	efficiency [dimensionless]
φ	generic variable (Eq. (19))
θ	inclination angle with respect to the horizontal [rad]
μ	dynamic viscosity [Pa s]
ρ	density [kg/m^3]
ρ_o	surface reflectivity [dimensionless]
σ	Stefan–Boltzman constant [5.6697×10^{-8} W/(m^2 K^4)]
τ	cover transmittance [dimensionless]
τ_w	shear stresses [N/m^2]
ξ	tube roughness [m]
Δp	pressure drop [Pa]
Δz	spatial discretization step [m]
Δt	temporal discretization step [s]
Φ	two-phase frictional multiplier $(\tau_w/(\tau_w)_{\text{liquid\_only}})$ [dimensionless]

Subscripts

amb	ambient
atm	atmospheric
b	beam
c	cover
conv	convective
eff	effective
ext	external
f	fluid
g	gas phase
i	internal tube
int	internal
l	liquid phase
op	optical
r	receiver
rad	radiative
th	thermal
tp	two-phase
w, e, n, s	neighbors (west, east, north, south)

Superscripts

*	guessed values
$^-$	arithmetical average over a CV
$^\sim$	integral average over a CV
^{o}	value of previous instant

$[X]_j^{j+1} = X_{j+1} - X_j$

carried out. The governing equations (continuity, momentum, and energy) inside the solar PTC receiver tube, together with the energy equation in the tube wall and cover wall and the thermal analysis in the solar concentrator were solved iteratively in a segregated manner. Secondly, the numerical model has been carefully validated with experimental data obtained by Sandia National Laboratories for single-pass solar PTC with air and vacuum in the space between receiver and cover. Finally, the model has been extended in order to simulate solar PTC with counter flow concentric circular heat exchangers (double-pass) and it has been demonstrated numerically that it can enhance the thermal efficiency compared with a single-pass device.

2. Mathematical formulation

The fluid enters into the receiver tube with a specific temperature (in the case of single phase flow) or quality (in the case of two-phase flow), pressure and mass flow rate. The receiver tube receives a useful energy gain ($\dot{q}_u$) of the sun. Finally, fluid exits the receiver with a pressure and temperature (in the case of single phase flow) or quality (in the case of two-phase flow) according to the boundary conditions found along the system.

A computational algorithm has been carried out in order to obtain the performance of a single-pass solar PTC with air or vacuum

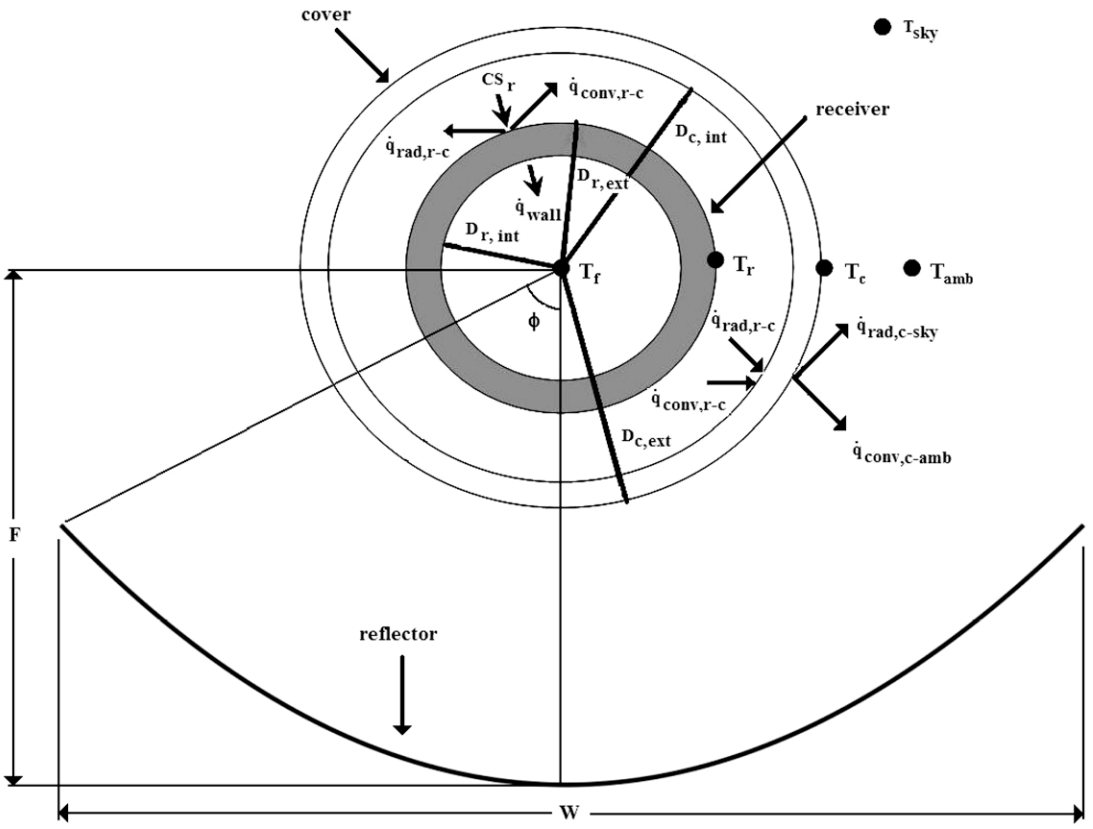

Fig. 1. Heat transfer nomenclature for a single-pass solar PTC.

in the space between the receiver and cover (Fig. 1). The numerical model was divided in four subroutines: fluid flow inside the receiver tube, heat transfer in the receiver wall tube, heat transfer in the glass cover and solar thermal analysis.

The following assumptions have been made in the mathematical model:

- The solar PTC has a tracking system that perfectly follows the sun during the day.
- The concentrator surface is specularly reflecting.
- One dimensional flow.
- Constant diameters and concentrator surfaces.
- Negligible conduction losses at the ends of each trough.

2.1. Solar thermal analysis

For a solar PTC, the incident solar radiation absorbed per unit of area by the receiver tube is [8]:

$$S_r = I_b \rho_o \tau \alpha \gamma F_a \tag{1}$$

The solar PTC optical efficiency is defined in the following form:

$$\eta_{op} = \frac{S_r}{I_b} \tag{2}$$

The aperture angle is defined as (see Fig. 1):

$$\phi = \tan^{-1}\left[\frac{8\frac{F}{W}}{16\left[\frac{F}{W}\right]^2 - 1}\right] \tag{3}$$

The minimum diameter required in the receiver tube in order to intercept the entire reflected ray is calculated in the following form [8]:

$$D = \frac{W \sin 0.267}{\sin \phi} \tag{4}$$

The concentration ratio is defined by:

$$C = \frac{W - D_{r,ext}}{\pi D_{r,ext}} \tag{5}$$

The useful energy gain per unit of receiver area ($\dot{q}_u$), expressed in terms of the local receiver temperature (T_r), cover temperature (T_c) and the incident solar radiation absorbed per unit of area by the receiver tube (S_r) is given by Duffie and Beckman [8]:

$$\dot{q}_u = CS_r - \left(h_{conv,r-c} + h_{rad,r-c}\right)(T_r - T_c) \tag{6}$$

The useful energy gain depends on both solar radiation absorbed by the receiver tube and thermal losses with the surroundings.

The radiative heat transfer coefficient between the receiver tube and cover is expressed by Duffie and Beckman [8] in the following formula:

$$h_{rad,r-c} = \frac{\sigma\left(T_r^2 + T_c^2\right)(T_r + T_c)}{\frac{1-\varepsilon_r}{\varepsilon_r} + \frac{1}{F_{rc}} + \frac{(1-\varepsilon_c)D_{r,ext}}{\varepsilon_c D_{c,int}}} \tag{7}$$

where view factor between the receiver and cover (F_{rc}) is considered equal to 1.

Natural heat transfer convection in a non-evacuated annular space gap for horizontal concentric cylinders can be estimated by the following correlations [9]:

$$\frac{k_{eff}}{k_{air}} = 0.317(Ra^*)^{1/4} \tag{8}$$

where

$$(Ra^*)^{1/4} = \left[\frac{\ln\left(D_{c,int}/D_{r,ext}\right)}{b^{3/4}\left(1/D_{r,ext}^{3/5} + 1/D_{c,int}^{3/5}\right)^{5/4}}\right] Ra^{1/4} \tag{9}$$

in which $b = (D_{c,int} - D_{r,ext})/2$ and the Rayleigh number, Ra, is based on the temperature differences in the annular space and the characteristic length b. The relation between the heat transfer coefficient $h_{conv,r-c}$ and the effective thermal conductivity, k_{eff}, is given by:

$$h_{conv,r-c} = \frac{2k_{eff}}{D_{r,ext}\ln(D_{c,int}/D_{r,ext})} \tag{10}$$

In the case of vacuum in the annular space between receiver and cover $h_{conv,r-c}$ is considered equal to zero.

The solar PTC global thermal efficiency is defined in the following form:

$$\eta_{th} = \frac{\dot{Q}_u}{A_{ref} I_b} \tag{11}$$

2.2. Fluid flow inside the receiver tube

The mathematical formulation of two-phase flow is evaluated inside a fluid characteristic control volume (CV) of a tube (Fig. 2a), where 'j' and '$j + 1$' represent the inlet and outlet sections, respectively.

Using as reference the geometry of the receiver tube (diameter, length, roughness and angle), the governing equations have been integrated assuming the following:

- One-dimensional fluid flow: $p(z,t)$, $H(z,t)$, $T(z,t)$, etc.
- Axial heat conduction inside the fluid is neglected.
- Separated flow model.
- Constant internal diameter and uniform surface roughness.

The general semi-integrated governing equations over the above mentioned finite *CV*, have the following form [10]:

Continuity:

$$[\dot{m}]_j^{j+1} + \frac{\partial m}{\partial t} = 0 \tag{12}$$

Momentum:

$$\left[\dot{m}_g v_g\right]_j^{j+1} + [\dot{m}_l v_l]_j^{j+1} + \Delta z \frac{\partial \tilde{\dot{m}}}{\partial t} = -[p]_j^{j+1} A_t - \tilde{\tau}_w P \Delta z - mg\sin\theta \tag{13}$$

Energy:

$$\left[\dot{m}_l e_l + \dot{m}_g e_g\right]_j^{j+1} + \frac{\partial\left(\bar{m}_l \bar{e}_l + \bar{m}_g \bar{e}_g\right)}{\partial t} - A_t \Delta z \frac{\partial \tilde{p}}{\partial t} = \sum \dot{Q} \tag{14}$$

where $e = H + v^2/2 + gz\sin\theta$.

The evaluation of the shear stresses are carried out by means of the friction factor (fr) and a two-phase multiplier (Φ) which are included in the following expression for wall shear stress: $\tau_w = \Phi(fr/4)(\dot{m}^2/2\rho_{tp}A_t^2)$. The one-dimensional model also requires knowledge of the two-phase flow structure (if two-phase flow exists), which is evaluated by means of the void fraction (ε_g) and the heat transfer through the tube wall and the fluid temperature are related by the convective heat transfer coefficient (h).

2.2.1. Evaluation of empirical coefficients

The mathematical model requires some additional local information, generally obtained from empirical correlations. After comparing different empirical correlations presented in the technical literature, the following ones have been selected:

2.2.1.1. Single phase region (subcooled liquid or superheated vapor). The Gnielinski correlation [11] is used to calculate the heat transfer coefficient:

$$Nu = \frac{(f/8)(Re - 1000)Pr}{1 + 12.7\sqrt{(f/8)}(Pr^{2/3} - 1)}; \tag{15}$$

where $f = (1.82\log_{10}Re - 1.64)^{-2}$

and the friction factor is evaluated from the expression proposed by Churchill [12]:

$$fr = 2\left[\left(\frac{8}{Re}\right)^{12} + \frac{1}{(A+B)^{3/2}}\right]^{1/12} \tag{16}$$

where

$$A = \left\{2.457\ln\left[1.0\Big/\left[\left(\frac{7}{Re}\right)^{0.9} + 0.27\frac{\xi}{D}\right]\right]\right\}^{16}. \tag{17}$$

$$B = \left(\frac{37530}{Re}\right)^{16} \tag{18}$$

2.2.1.2. Equilibrium two-phase region (if it exists). In the two-phase flow region, the void fraction is estimated from the equation of Rouhani and Axelsson [13]. For the convective heat transfer coefficient, the boiling flow model proposed by Zürcher et al. [14] is applied. The friction factor is calculated from the same equation as in the case of subcooled liquid phase using a two-phase frictional multiplier according to Friedel [15].

Temperature, mass fraction and all the thermophysical properties are calculated using matrix functions of the pressure and enthalpy obtained using REFPROP v7.0 [16] (for air and water) and for silicone-base fluid (thermal oil) from data given by the manufacturer [17], i.e.:

$$\varphi = \varphi(p,H) \quad \text{where} \quad \varphi = T, x_g, \rho, \ldots \tag{19}$$

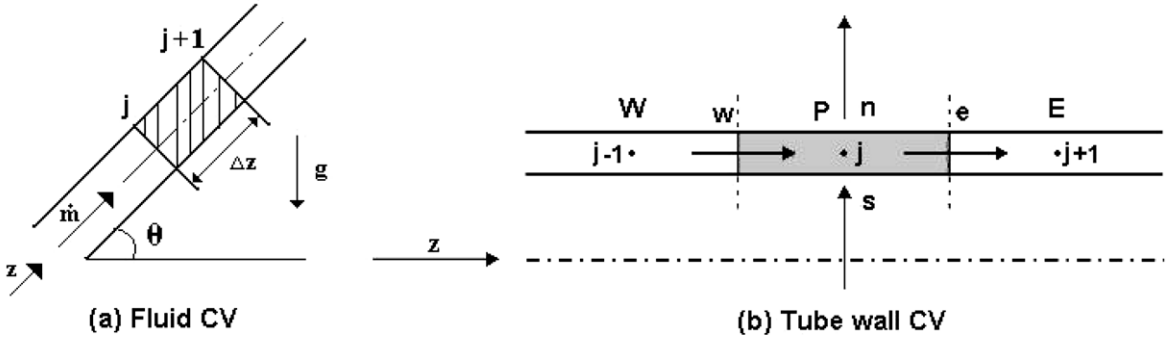

Fig. 2. Characteristics CV: (a) fluid CV and (b) tube wall CV.

2.2.2. Fluid flow analysis

The numerical analysis is carried out in terms of a CV method. The discretized equations are coupled using a fully implicit step-by-step method in the flow direction. From the known values at the inlet section and the wall boundary conditions, the variable values at the outlet of each CV are iteratively obtained from the discretized governing equations. Outlet values are the inlet values for the next CV. The procedure is carried out until the end of the receiver tube is reached.

For each *CV*, a set of algebraic equations is obtained by a discretization of the governing Eqs. (12)–(14) to obtain the value of the dependent variable (mass flow rate, pressure and enthalpy) at the outlet section of each CV.

The outlet mass flow rate is obtained from the discretized *continuity equation* (Eq. (12)),

$$\dot{m}_{j+1} = \dot{m}_j - \frac{A_t \Delta z}{\Delta t}\left(\bar{\rho}_{tp} - \bar{\rho}^o_{tp}\right) \tag{20}$$

where the two-phase density is obtained from: $\rho_{tp} = \varepsilon_g \rho_g + (1-\varepsilon_g)\rho_l$.

In terms of the mass flow rate, gas and liquid velocities are calculated as,

$$v_g = \left[\frac{\dot{m}x_g}{\rho_g \varepsilon_g A_t}\right]; v_l = \left[\frac{\dot{m}(1-x_g)}{\rho_l(1-\varepsilon_g)A_t}\right] \tag{21}$$

The discretized *momentum equation* (Eq. (13)) is solved for the outlet pressure,

$$p_{j+1} = p_j - \frac{\Delta z}{A_t}\left(\Phi \bar{f} r \pi D_{r,int}\frac{\bar{\dot{m}}^2}{8\bar{\rho}_{tp}A_t^2} + \bar{\rho}_{tp}A_t g \sin\theta + \frac{\left[\dot{m}\left(x_g v_g + (1-x_g)v_l\right)\right]_j^{j+1}}{\Delta z} + \frac{\bar{\dot{m}} - \bar{\dot{m}}^o}{\Delta t}\right) \tag{22}$$

From the *energy equation* (Eq. (14)) and the *continuity equation* (Eq. (12)), the following equation is obtained for the outlet enthalpy:

$$H_{j+1} = \frac{2\dot{q}_{wall}\pi D_{r,int}\Delta z - \dot{m}_{j+1}a1 + \dot{m}_j a2 + \frac{A_t \Delta z}{\Delta t}a3}{\dot{m}_{j+1} + \dot{m}_j + \bar{\rho}^o_{tp}A_t \Delta z/\Delta t} \tag{23}$$

where

$$a1 = (x_g v_g + (1-x_g)v_l)^2_{j+1} + g\sin\theta\Delta z - H_j \tag{24}$$

$$a2 = (x_g v_g + (1-x_g)v_l)^2_{j} - g\sin\theta\Delta z + H_j \tag{25}$$

$$a3 = 2\left(\bar{p}_j - \bar{p}^o_j\right) - \bar{\rho}^o_{tp}\left(H_j - 2\overline{H}^o_j\right) - \left(\bar{\rho}\bar{v}^2_j - \bar{\rho}^o\bar{v}^{o^2}_j\right) \tag{26}$$

The above mentioned equations of mass, momentum and energy are applicable to transient two-phase flow. Situations of steady flow and/or single-phase flow (subcooled liquid or superheated vapor) are particular cases of this formulation. Moreover, the mathematical formulation in terms of enthalpy gives generality of the analysis, because only one equation is needed for all the regions and gives opportunity for easily dealing with cases of mixtures of fluids.

2.3. Receiver tube wall

The conduction equation has been written assuming one-dimensional transient temperature distribution (the radiant flux is not uniform at 360° around the receiver however due to the small receiver tube diameter and the tube thermal conductivity a one-dimensional temperature distribution has been assumed).

A characteristic tube wall CV is shown in Fig. 2b, where *P* represents the central node, *E* and *W* indicate its neighbors. The CV-faces are indicated by *e*, *w*, *n* and *s*. Integrating the conduction equation over this CV, the following equation is obtained:

$$\left(\tilde{\dot{q}}_{wall}\pi D_{r,int} - \tilde{\dot{q}}_u \pi D_{r,ext}\right)\Delta z + \left(\tilde{\dot{q}}_w - \tilde{\dot{q}}_e\right)A_{t,r} = m\frac{\partial \widetilde{H}}{\partial t} \tag{27}$$

where $\tilde{\dot{q}}_{wall} = h_f(T_r - T_f)$, and the conductive heat fluxes are evaluated using the Fourier law:

$$\tilde{\dot{q}}_e = -k_e\left(\frac{\partial T_r}{\partial z}\right)_e; \tilde{\dot{q}}_w = -k_w\left(\frac{\partial T_r}{\partial z}\right)_w \tag{28}$$

Substituting their respective heat fluxes and rearrangement Eq. (27), the following equation has been obtained for each node of the grid:

$$a_j T_{r,j} = b_j T_{r,j+1} + c_j T_{r,j-1} + d_j \tag{29}$$

where the coefficients are:

$$a_j = b_j + c_j + h_{f,j}\pi D_{r,int}\Delta z + \frac{A_{t,r}\Delta z}{\Delta t}\rho c_p \quad b_j = \frac{k_e A_{t,r}}{\Delta z} \quad c_j = \frac{k_w A_{t,r}}{\Delta z}$$

$$d_j = \left(h_{f,j}\pi D_{r,int}\overline{T}_{f,j} + \dot{q}_{u,j}\pi D_{r,ext}\right)\Delta z + \frac{A_{t,r}\Delta z}{\Delta t}\rho c_p T^o_{r,j}$$

The coefficients mentioned above are applicable for $2 \leqslant j \leqslant n_z - 1$; for $j = 1$ and $j = n_z$ adequate coefficients are used taking into account the axial heat conduction or temperature boundary conditions. The set of heat conduction discretized equations is solved using the TDMA algorithm [18].

2.4. Cover tube wall

The same procedure mentioned above for the receiver tube wall has been used. Integrating the conduction equation over the cover tube wall CV, the following equation is obtained as result:

$$\left(\tilde{\dot{q}}_s \pi D_{r,ext} - \tilde{\dot{q}}_n \pi D_{c,ext}\right)\Delta z + \left(\tilde{\dot{q}}_w - \tilde{\dot{q}}_e\right)A_{t,c} = m\frac{\partial \widetilde{H}}{\partial t} \tag{30}$$

$\tilde{\dot{q}}_e$ and $\tilde{\dot{q}}_w$ are evaluated using the Fourier law and:

$$\tilde{\dot{q}}_s = \tilde{\dot{q}}_{conv,r-c} + \tilde{\dot{q}}_{rad,r-c} = (h_{conv,r-c} + h_{rad,r-c})(T_r - T_c) \tag{31}$$

$$\tilde{\dot{q}}_n = \tilde{\dot{q}}_{conv,c-amb} + \tilde{\dot{q}}_{rad,c-sky} = h_{conv,c-amb}(T_c - T_{amb}) + h_{rad,c-sky}(T_c - T_{sky}) \tag{32}$$

where

$$T_{sky} = 0.0552T^{1.5}_{amb} \tag{33}$$

$$h_{rad,c-sky} = \varepsilon_c \sigma\left(T^2_{sky} + T^2_c\right)(T_{sky} + T_c) \tag{34}$$

And according to Karlekar and Desmond [19]:

$$h_{conv,c-amb} = 0.989Re^{0.33}Pr^{1/3}\frac{k_{air}}{D_{c,ext}} \quad \text{for} \quad 0.4 < Re \leqslant 40 \tag{35}$$

$$h_{conv,c-amb} = 0.683Re^{0.486}Pr^{1/3}\frac{k_{air}}{D_{c,ext}} \quad \text{for} \quad 40 < Re \leqslant 4000 \tag{36}$$

$$h_{conv,c-amb} = 0.193Re^{0.618}Pr^{1/3}\frac{k_{air}}{D_{c,ext}} \quad \text{for} \quad 4000 < Re \leqslant 40,000 \tag{37}$$

$$h_{conv,c-amb} = 0.0266Re^{0.805}Pr^{1/3}\frac{k_{air}}{D_{c,ext}} \quad \text{for} \quad 40,000 < Re \leqslant 400,000 \tag{38}$$

Finally, $h_{conv,c-amb}$ is taken as the maximum value between one of its corresponding above correlation and the following correlation for natural convention around cylinders developed by Churchill and Chu [20]:

$$h_{conv,c-amb} = \left(0.6 + 0.387\left(\frac{Ra}{\left(1 + \left(\frac{0.559}{Pr}\right)^{9/16}\right)^{16/9}}\right)^{1/6}\right)^2 \frac{k_{air}}{D_{c,ext}} \tag{39}$$

3. Numerical solution of single-pass solar PTC

The solution process is carried out on the basis of a global algorithm (programmed in C language) that solves in a segregated manner the fluid flow inside the receiver tube, the heat conduction in the receiver tube wall, the heat conduction in the cover tube wall and the solar PTC thermal analysis. The coupling between the four main subroutines is performed iteratively following the procedure described below (see Fig. 3):

1. *For fluid flow inside the receiver tube*, the equations are solved considering the receiver tube wall temperature distribution as a boundary condition, and evaluating the temperature and the convective heat transfer coefficient in each fluid CV.
2. *In the receiver tube wall*, the temperature distribution is re-calculated using the fluid flow temperature and the convective heat transfer coefficient evaluated in the preceding step, and considering the useful energy gain as boundary condition.
3. *In the cover tube wall*, the temperature distribution is calculated using the receiver tube wall, ambient and sky temperatures and the convective and radiative heat transfer coefficients between the cover and receiver and cover and sky and ambient.

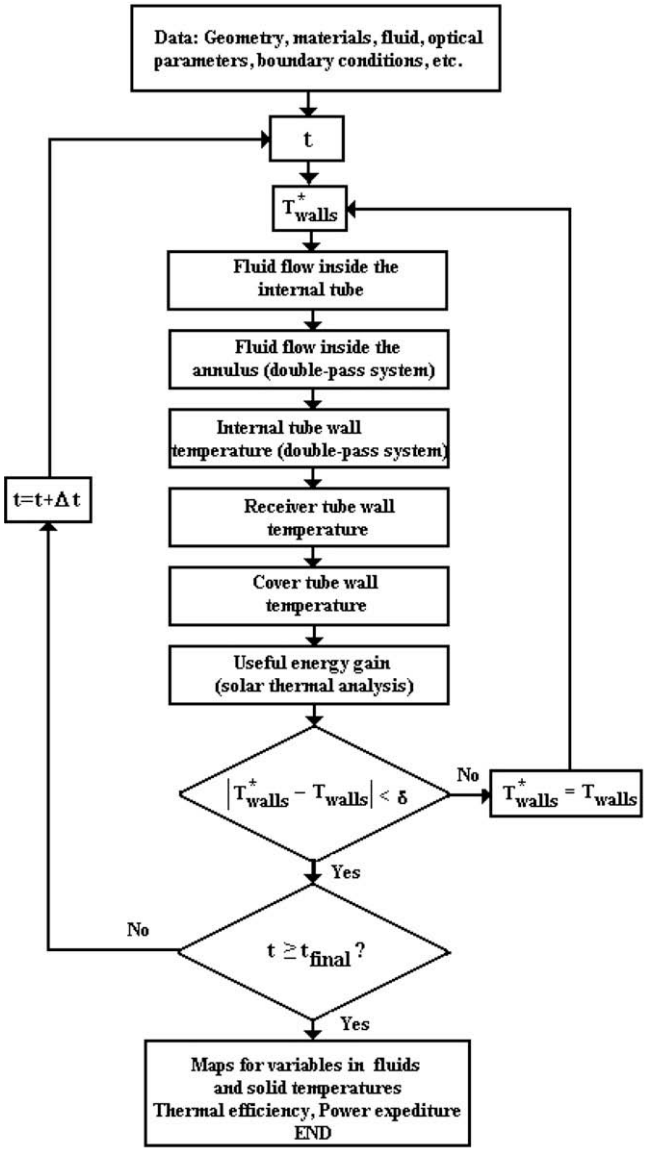

Fig. 3. Numerical algorithm flow diagram.

4. *The useful energy gain* is obtained in terms of the thermal analysis carried out on the solar PTC, and the receiver tube and cover temperature distributions calculated in the previous steps.

The governing equations corresponding to a steady state situation are the same equations developed without considering the temporal derivative terms. The global convergence is reached when in two consecutive loops of the four main subroutines; a strict convergence criterion is verified for all the CVs in the domain (for more detail [10]).

4. Single-pass solar PTC model validation

In order to validate the numerical model developed a comparison with the experimental data obtained by Sandia National Laboratories for a single-pass solar PTC with air and vacuum in the space between the receiver and cover working with a single-phase water and syltherm 800 oil (silicone-based fluid) under different working conditions [2] has been carried out. Cermet a graded ceramic/metal selective surface coating to the steel receiver by a vacuum sputtering process was used in the experimental tests. The detailed solar PTC specifications are given in Table 1. Due to the AZTRAK rotating platform of Sandia National Laboratories is an azimuth-tracking platform, it can position a collector at zero incident angle (radiation normal incident to the plane of aperture, $F_a = 1$) at any hour of any day. The experimental test reported at zero incident angle have been using for comparison in this paper.

Validation of air and vacuum between receiver and cover is due to most of the design systems are vacuum ones but accidents during operation can produce vacuum lost or the glass envelope can be broken. Moreover air between receiver and cover technology is cheaper than vacuum systems. All the numerical results presented in this paper have been obtained using 300 CVs to get grid-independent solutions.

4.1. Air between receiver and cover

The first validation was against the single-pass experimental thermal losses from the receiver with air in the space between the receiver and cover as a function of operating temperature. Experimentally, good thermal loss data is more difficult to obtain than heat gain (efficiency) data, because the temperature change across the receiver is smaller by as much as an order of magnitude. A true measure of receiver thermal loss with zero contribution due to direct or scattered light absorption by the receiver can be

Table 1
Solar PTC specifications [2] used in the model validation

Receiver length (L)	7.8 m
Collector width (W)	5 m
Focal distance (F)	1.84 m
Receiver internal diameter ($D_{r,int}$)	0.066 m
Receiver external diameter ($D_{r,ext}$)	0.070 m
Receiver tube thermal conductivity (k_r)	54 W/m K
Glass cover internal diameter ($D_{c,int}$)	0.115 m
Glass cover external diameter ($D_{c,ext}$)	0.109 m
Concentration ratio (C)	22.42
Receiver absorptance (α)	0.906
Receiver emittance (ε_r)	0.14
Glass cover transmittance (τ)	0.95
Reflected surface reflectivity (ρ_o)	0.93
Shape factor (γ)	0.92
Inclination angle (θ)	0.0
Incident angle modifier (F_a)	1.0
Optical efficiency (η_{op})	0.736
Atmospheric pressure (Albuquerque) (p_{atm})	86 kPa

obtained by aiming the reflector at a clear sky, at night. Other tests have also shown that an equivalent loss value occurs during more normal daylight hours when the receiver is shaded from direct sunlight and the reflector is aimed at a clear sky (this experimental procedure was used by Sandia National Laboratories). The experimental error band reported on the data points are the expected worst-case errors caused by the measuring instruments [2]. The single-pass solar PTC numerical model comparison of the performance against experimental data is shown in Fig. 4a, the agreement here is very good; the model and test data essentially agree, within the bounds of experimental uncertainty, over the entire temperature range.

The second validation was against experimental measurements of zero incident angle efficiency made with water and oil at approximately ambient-air temperature, and at approximately 50 °C intervals up to 400 °C. The near ambient-air temperature measurement was used to define the approximate optical efficiency of the solar PTC (0.736). The higher temperature efficiency measurements document the decrease in efficiency caused by increasing thermal losses as the operating temperature is increased. The comparison of the performance between the numerical model developed and the experimental data is shown in Table 2. A good degree of correlation has been obtained for 11 data points evaluated for thermal efficiency of a single-pass solar PTC with air between receiver and cover, the maximum error is 6.02% with a mean deviation of ±2.59%. For the increment of temperature in the fluid: the maximum error is 5.99% or 1.07 °C with a mean deviation of ±2.52% or ±0.43 °C.

4.2. Vacuum between receiver and cover

In these cases, the numerical model considered that the natural heat transfer convection in the annular space between receiver and cover is negligible ($h_{conv,r-c} = 0$). A comparison between the single-pass solar PTC numerical model against thermal losses experimental data is shown in Fig. 4b, the model and test data essentially agree, within the bounds of experimental uncertainty, over the entire temperature range (temperature change across the receiver is smaller than in the case of air between receiver and cover, for this reason higher uncertainties are expected).

A comparison between the numerical model developed and the experimental data for a single-pass solar PTC with vacuum between receiver and cover is shown in Table 3. A good degree of correlation has been obtained for 9 data points evaluated for thermal efficiency; the maximum error is 2.84% with a mean deviation of ±1.79%. For the increment of temperature in the fluid: the maximum error is 3.24% or 0.64 °C with a mean deviation of ±1.98% or ±0.39 °C. Comparison between air and vacuum in the space between receiver and cover show that elevated temperature performance is significantly degraded by increasing thermal losses when air fills this space.

The numerical model is based on the applications of governing equations and used general empirical correlations; for this reason, it is possible to make use of it with greater confidence to other fluids, mixtures and operating conditions (including two-phase flow); it allows using the model developed as an important tool to design and optimize these kinds of systems.

5. Solar PTC improvement using counter flow concentric circular heat exchangers (double-pass)

The recycle-effect concept is broadly used in absorption, fermentation, and polymerization industries. The effects of recycle in laminar flows have been widely studied in previous works. For example, the effects of recycle in laminar flows at the ends on the heat transfer through a concentric circular tube with uniform wall fluxes were studied analytically by Ho and Yeh [21]. The analytical model developed have the following assumptions: constant physical properties, uniform heat fluxes, fully developed laminar flow, negligible axial conduction and negligible thickness and thermal resistance in the impermeable tube. They demonstrated that the external recycle can enhance the heat transfer efficiency compared that with a single-pass device for laminar flows.

In general, numerical models are more accurate and general methods than analytical ones due to the governing equations are solved with fewer restrictions (for example, the model developed in this paper considers: variable physical properties, non uniform heat fluxes, axial conduction and thermal resistance in tubes, laminar and turbulent flow, etc.).

5.1. Mathematical formulation of double-pass device

A detailed numerical simulation of optical, thermal and fluid-dynamic behavior of a Solar PTC with counter flow concentric

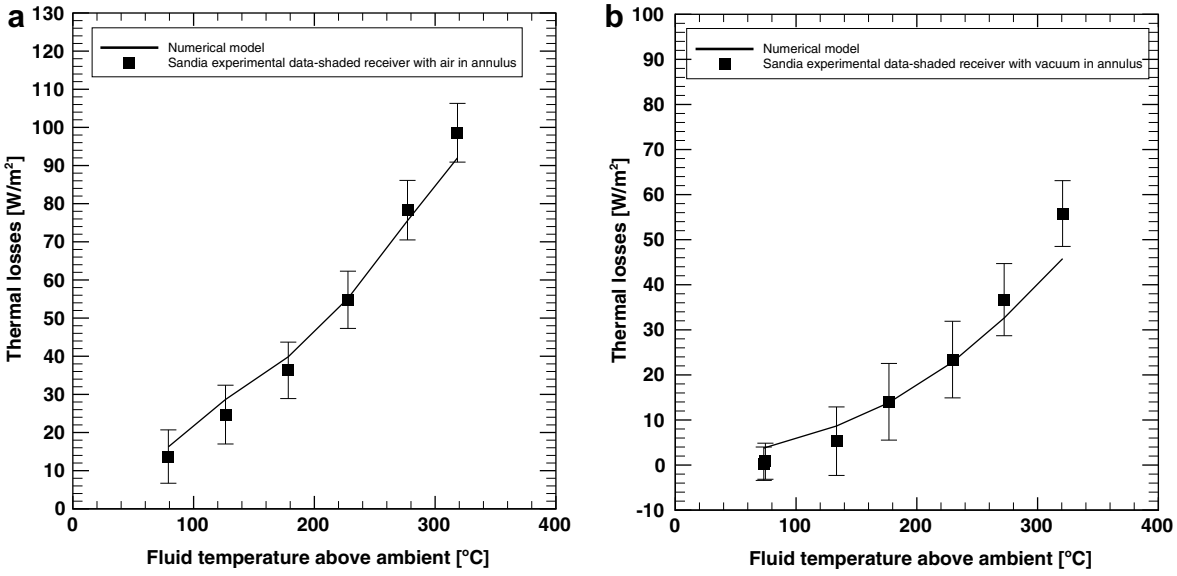

Fig. 4. Thermal losses comparison between Sandia experimental data and single-pass model developed for a shaded receiver with: (a) air between receiver and cover and (b) vacuum between receiver and cover. Error bars represent the measurement errors reported [2].

Table 2
Comparison between Sandia experimental data [2] for a single-pass solar PTC with air between receiver and cover and model developed

Case	Fluid	I_b (W/m^2)	Flow rate (1/min)	Wind speed (m/s)	T_{amb} (°C)	T_{inlet} (°C)	*exp* ΔT (°C)	Model ΔT (°C)	% Error *exp* vs model	*exp* η_{th} (%)	Model η_{th} (%)	% Error *exp* vs model
1	Water	925.1	20.7	3.4	38.4	29.5	17.8	18.04	1.36	73.68 ± 1.96	72.11	2.13
2	Oil	813.1	50.3	3.6	25.8	101.2	17.8	16.73	5.99	71.56 ± 2.21	67.25	6.02
3	Oil	858.4	52.9	3.1	27.6	154.3	17.4	16.64	4.36	69.20 ± 2.10	66.21	4.32
4	Oil	878.7	54.6	3.1	28.6	202.4	17.0	16.31	4.05	67.10 ± 1.88	64.60	3.73
5	Oil	896.4	55.2	0.9	30.0	250.7	17.1	16.57	3.08	65.50 ± 1.80	63.65	2.83
6	Oil	889.7	55.3	2.8	28.6	251.1	17.2	16.23	5.63	66.61 ± 2.29	62.89	5.58
7	Oil	906.7	55.4	0.0	31.7	299.5	17.0	16.94	0.36	62.58 ± 1.79	62.39	0.30
8	Oil	874.1	56.2	4.0	28.7	344.9	16.2	15.82	2.32	59.60 ± 2.27	58.56	1.75
9	Oil	870.4	56.1	0.6	29.1	345.5	16.1	16.11	0.08	59.40 ± 2.12	59.74	0.57
10	Oil	879.5	55.4	1.8	27.4	348.9	16.3	16.35	0.29	58.52 ± 2.02	58.99	0.81
11	Oil	898.6	56.2	2.8	29.7	376.6	16.5	16.47	0.19	56.54 ± 1.93	56.83	0.51
								Average	**2.52**		Average	**2.59**
								Max	**5.99**		Max	**6.02**

Table 3
Comparison between Sandia experimental data [2] for a single-pass solar PTC with vacuum between receiver and cover and model developed

Case	Fluid	I_b (W/m^2)	Flow rate (1/min)	Wind speed (m/s)	T_{amb} (°C)	T_{inlet} (°C)	*exp* ΔT (°C)	Model ΔT (°C)	% Error *exp* vs model	*exp* η_{th}	Model η_{th} (%)	% Error *exp* vs model
1	Water	807.9	18.4	1.0	15.8	18.3	17.8	17.79	0.23	72.63 ± 1.91	72.39	0.33
2	Oil	933.7	47.7	2.6	21.2	102.2	21.8	21.25	2.51	72.51 ± 1.95	70.69	2.51
3	Oil	968.2	47.8	3.7	22.4	151.0	22.3	22.94	2.86	70.90 ± 1.92	70.13	1.09
4	Oil	982.3	49.1	2.5	24.3	197.5	22.0	21.67	1.49	70.17 ± 1.81	69.32	1.21
5	Oil	909.5	54.7	3.3	26.2	250.7	18.7	18.19	2.75	70.25 ± 1.90	68.26	2.84
6	Oil	937.9	55.5	1.0	28.8	297.8	19.1	18.85	1.30	67.98 ± 1.86	67.40	0.86
7	Oil	880.6	55.6	2.9	27.5	299.0	18.2	17.61	3.24	68.92 ± 2.06	67.08	2.67
8	Oil	903.2	56.3	4.2	31.1	355.9	18.1	18.40	1.67	63.82 ± 2.36	65.19	2.15
9	Oil	920.9	56.8	2.6	29.5	379.5	18.5	18.83	1.77	62.34 ± 2.41	63.84	2.41
								Average	**1.98**		Average	**1.79**
								Max	**3.24**		Max	**2.84**

circular heat exchangers is carried out in the following sections based on the single-pass model previously developed and validated.

In this section, the numerical algorithm and the mathematical formulation to solve the internal tube wall and fluid flow inside the annulus included in the new numerical model is presented.

5.1.1. Spatial discretization

Fig. 5 shows half figures of the spatial discretization of two flow patterns of a solar PTC with counter flow concentric circular heat exchangers. The discretization nodes are located at the inlet and outlet sections of the CVs in the fluid flow zones, while the discretization nodes are centered in the CVs in the internal, receiver and cover tube wall. Each one of the fluids has been divided into n_z volumes (i.e., $n_z + 1$ nodes). The tube walls have been discretized into n_z control volumes of length Δz.

Under this design conditions (Fig. 5), for flow pattern A before entering the internal tube for a double-pass operations the fluid of mass flow rate ($\dot{m}$) and the inlet temperature (T_{in}) will mix with the fluid of mass flow rate ($M\dot{m}$) exiting the annulus channel. Counter current flow is achieved with the aid of conventional pump situated at the end of the inner channel and the mass flow rate then may be regulated. For flow pattern B, the inlet fluid may flow through the annulus with premixing the external recycle exiting from the inlet tube. In each flow pattern, the fluid is completely mixed at the inlet and outlet section of the tube.

5.1.2. Fluid flow inside the annulus

The same process developed for the fluid flow inside the receiver tube (Section 2.2) is carried out considering temperatures, area and roughness of both wall (internal and receiver tube wall).

The evaluation of empirical coefficients in this zone is as follow: the friction factor is evaluated from the expressions proposed by Churchill [12] (Eq. (16)) with the hydraulic diameter, the convective heat transfer coefficient is calculated using the Monrad and Pelton correlation developed specifically for flow in annulus (cited by Jakob [22]) that for the internal and external tube in the annulus are, respectively:

$$Nu = 0.02Re^{0.8}Pr^{1/3}\left(\frac{D_{r,int}}{D_{i,ext}}\right)^{0.53} \tag{40}$$

$$Nu = 0.027Re^{0.8}Pr^{1/3} \tag{41}$$

5.1.3. Heat conduction in the internal tube wall

The same process developed for the receiver tube wall (Section 2.3) is carried out considering one-dimensional transient temperature distribution and negligible heat exchanged by radiation.

Integrating the energy equation over the internal tube wall CV (Fig. 2b), the following equation is obtained:

$$\left(\tilde{\dot{q}}_s P_s - \tilde{\dot{q}}_n P_n\right)\Delta z + \left(\tilde{\dot{q}}_w - \tilde{\dot{q}}_e\right)A_t = m\frac{\partial \tilde{H}}{\partial t} \tag{42}$$

where $\tilde{\dot{q}}_s$ and $\tilde{\dot{q}}_n$ are evaluated using the respective convective heat transfer coefficient and fluid temperatures in each zone (fluid flow inside the internal tube and annulus), and the conductive heat fluxes are evaluated from the Fourier law, that is: $\tilde{\dot{q}}_e = -k_e(\partial T_{wall}/\partial z)_e$ and $\tilde{\dot{q}}_w = -k_w(\partial T_{wall}/\partial z)_w$.

Substituting their respective heat fluxes and rearrangement Eq. (42), the following equation has been obtained for each node of the grid:

$$a_j T_{wall,j} = b_j T_{wall,j+1} + c_j T_{wall,j-1} + d_j \tag{43}$$

where the coefficients are,

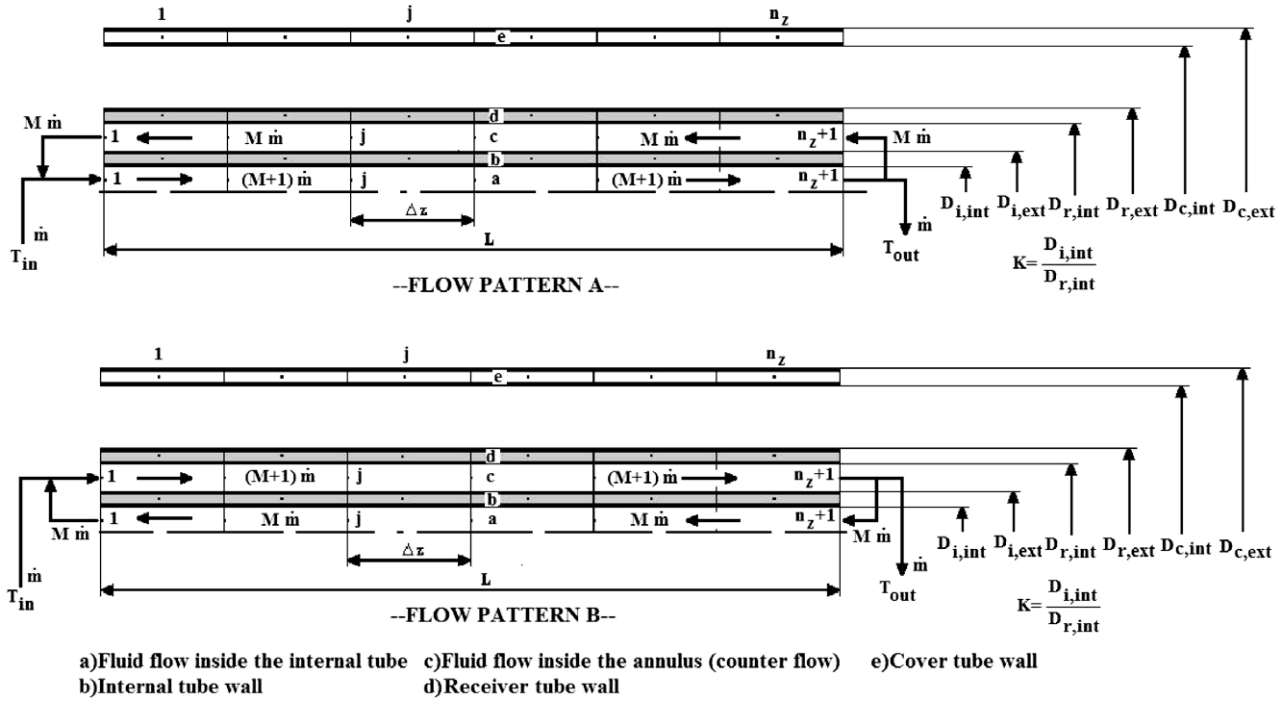

Fig. 5. Schematic diagram of half figures of double-pass concentric circular heat exchangers with external recycle at both ends. Flow pattern A: before entering the internal tube for a double-pass operations the fluid of mass flow rate ($\dot{m}$) and the inlet temperature (T_{in}) will mix with the fluid of mass flow rate ($M\dot{m}$) exiting the annulus channel. Flow pattern B: the inlet fluid may flow through the annulus with premixing the external recycle exiting from the inlet tube.

$$a_j = \frac{k_w A_t}{\Delta z} + \frac{k_e A_t}{\Delta z} + (h_s P_s + h_n P_n)\Delta z + \frac{A_t \Delta z}{\Delta t}\rho c_p \quad b_j = \frac{k_e A_t}{\Delta z}$$

$$c_j = \frac{k_w A_t}{\Delta z} \quad d_j = (h_s P_s \overline{T}_s + h_n P_n \overline{T}_n)\Delta z + \frac{A_t \Delta z}{\Delta t}\rho c_p T^o_{wall,j}$$

The coefficients mentioned above are applicable for $2 \leqslant j \leqslant n_z - 1$; for $j = 1$ and $j = n_z$ adequate coefficients are used to take into account the axial heat conduction or temperature boundary conditions. The set of heat conduction discretized equations is solved using the algorithm TDMA [18].

5.2. Numerical solution of a double-pass solar PTC

At each time step solution process is carried out on the basis of a global algorithm (programmed in C language) that solves in a segregated manner the flow inside the internal tube, the flow inside the annulus and the heat conduction in the internal tube wall, the receiver tube wall, and the cover tube wall and finally the solar PTC thermal analysis. The coupling between the six main subroutines has been performed iteratively each time step following the procedure (see Fig. 3):

- *For fluid flow inside the internal tube*, the equations are solved considering the internal tube wall temperature distribution as boundary condition, and evaluating the convective heat transfer and fluid temperatures in each CV.
- *For fluid flow inside the annulus*, the same process is carried out considering both wall temperatures and roughness (internal tube wall and receiver tube wall).
- *In the internal tube wall*, the temperature distribution is re-calculated using the fluid flow temperature and the convective heat transfer coefficients evaluated in the preceding steps.
- *In the receiver tube wall*, the temperature distribution is re-calculated using the fluid flow temperature and the convective heat transfer coefficient evaluated in the fluid flow inside the annulus, and considering the useful energy gain as boundary condition.
- *In the cover tube wall*, the temperature distribution is calculated using the receiver tube wall, ambient and sky temperatures and the convective and radiative heat transfer coefficients between the cover and receiver and cover and sky and ambient.
- *The useful energy gain* is obtained in terms of the thermal analysis carried out on the solar PTC, and the receiver tube and cover temperature distributions calculated in the previous steps.

The global convergence is reached when in two consecutive loops of the six main subroutines; a strict convergence criterion is verified for all the CVs in the domain.

5.3. Numerical results of a double-pass solar PTC

In Section 4, the single-pass solar PTC numerical model has been carefully validated with experimental data obtained by Sandia National Laboratories [2] for air and vacuum between receiver and cover under different working conditions. In this section, the improvement using counter flow concentric circular heat exchangers for flow patterns A and B (Fig. 5) are evaluated using the same PTC specifications given in Table 1 and those ones given specifically for a double-pass solar PTC (Table 4). The boundary conditions of case 11 (Table 2) with air and case 9 (Table 3) with vacuum in the space between receiver and cover have been selected as validated cases due to they have the highest thermal losses and hence the lower global thermal efficiencies.

Parameters used in the cases evaluated numerically are: the solar PTC global thermal efficiency (Eq. (11)); Reynolds number ($Re = 4\dot{m}/\pi D_{r,int}\mu$); the channel thickness ratio ($K = D_{i,int}/D_{r,int}$); and the recycle ratio (M).

The improvement of solar PTC performance (I_D) and the total friction power expenditure (P_T) [23] are used as other performance parameters, which are calculated in the following form:

Table 4
Solar PTC specifications used for the double-pass device

	Case 11, Table 2 (air between receiver and cover)	Case 9, Table 3 (vacuum between receiver and cover)
Solar beam irradiance (I_b) [W/m^2]	898.6	920.9
Wind speed [m/s]	2.8	2.6
Ambient temperature (T_{amb}) [°C]	29.7	29.5
Inlet temperature (T_{inlet}) [°C]	376.6	379.5
Reynolds number (Re)x10^3	20, 40, 60, 80, 100	17, 37, 57, 77, 97
Internal tube diameters ($D_{i,int}$, $D_{i,ext}$) [mm][a]	(22.45, 26.67) (36.62, 42.16) (54.79, 60.33)	(22.45, 26.67) (36.62, 42.16) (54.79, 60.33)
Channel thickness ratio (K)	0.34, 0.55, 0.83	0.34, 0.55, 0.83
Recycle ratio (M)	0.5, 1.0, 2.0	0.5, 1.0, 2.0

[a] Commercial tubes available in stainless steel.

$$I_D = \frac{\eta_{th,new} - \eta_{th,reference}}{\eta_{th,reference}} \times 100 \quad (44)$$

$$P_T = \frac{\dot{m}_1 \Delta p_1}{\bar{\rho}_1} + \frac{\dot{m}_2 \Delta p_2}{\bar{\rho}_2} \quad (45)$$

where subscript 1 and 2 indicate the flow inside the internal tube and annulus, respectively. In the case of single-pass only the first term appears.

5.3.1. Case of air between receiver and cover (double-pass device)

According to Fig. 6, the desirable effects of increases heat transfer and reducing surrounding thermal losses increases when the recycle ratio (M), channel thickness ratio (K) and Reynolds number rise. The reason why the desirable effect increasing when increasing the channel thickness ratio may be considered as the enhancement of convective heat transfer rate due to increasing the flow velocity in the annular channel, where the fluid is heated, is more effective than that in the inner channel. The validated case shown is the case 11 (Table 2).

A comparison of flow patterns A and B in Fig. 6 indicates an enhancement of global thermal efficiency occurs for flow pattern B with design and operation parameters. The reason is again due to flow velocities in the annular channel are higher in flow pattern B than flow pattern A, that high flows are more effective that in the inner channel.

Fig. 7 shows that improvement of solar PTC performance for flow pattern B is obtained if the solar PTC is operated with a double-pass device in which the enhancement of convective heat transfer coefficient is provided. The advantages are evident with small Reynolds number and diminished when Reynolds number is increased. However for the validated case (case 11, Table 2) the improvement of solar PTC performance with a double-pass device and the same Reynolds number can be of approximately 3.2% and for lower Reynolds number this value can be higher than 10%.

The friction power expenditure increment calculated for the double-pass device is evident in Fig. 7; these values can be increased up to 2 to 3 orders of magnitude compared with the single-pass device. However, they can be still small because the friction power expenditure can be as small as 0.05 W for the validated case (single-pass). Losses of hundreds watts could be small in comparison with the energy gain by the fluid in the order of thousands of watts. The enhancement of heat transfer accompanies increase of hydraulic dissipated energy to maintain the extra

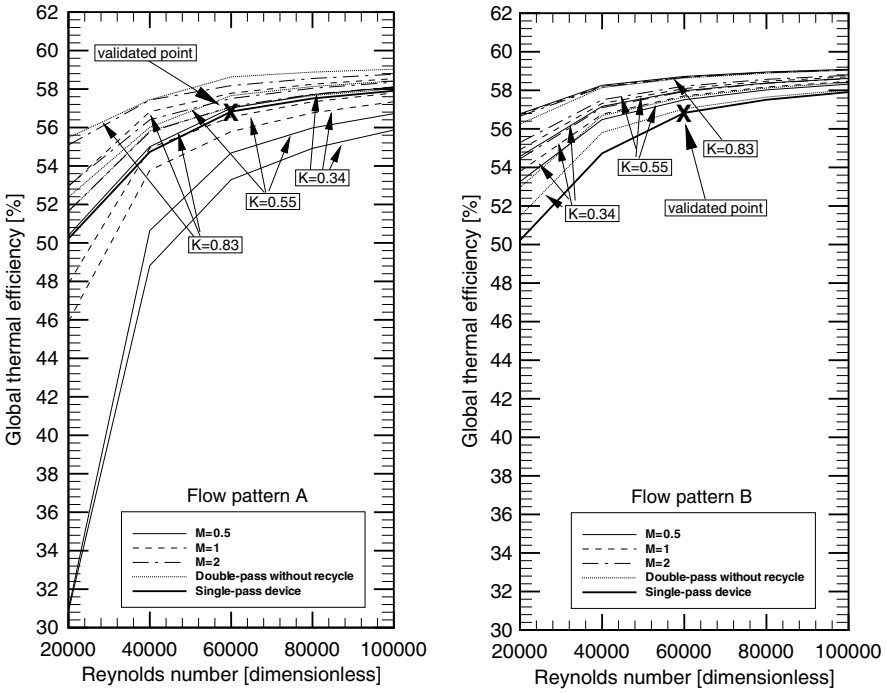

Fig. 6. Global thermal efficiency for a solar PTC with air between receiver and cover vs. Re with K and M as parameters (flow pattern A and B). Validated case (case 11, Table 2).

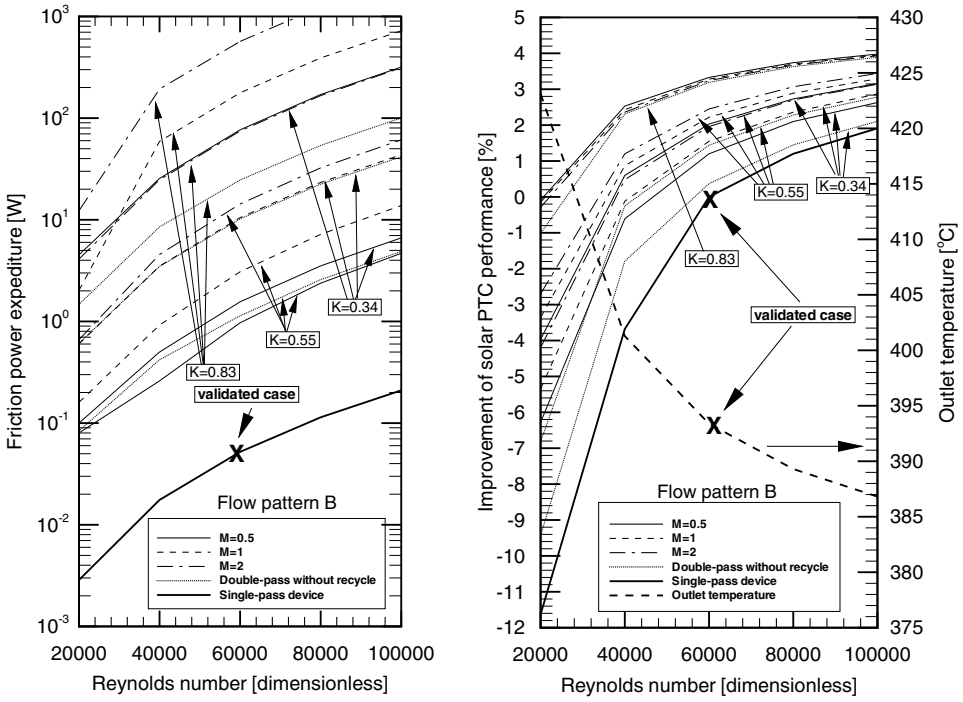

Fig. 7. Friction power expenditure, improvement and outlet temperature for a solar PTC with air between receiver and cover vs. *Re* with *K* and *M* as parameters (flow pattern B). Validated case (case 11, Table 2).

friction loss. The evaluation of economical sense including the operating cost in the double-pass heat exchanger is necessary before take a decision to construct a solar PTC with counter flow concentric circular heat exchangers with or without recycle. However, the heat transfer advantage of the present double-pass devices under the same design and operating parameter is evident as compared with those in the single-pass device.

In Fig. 8, the receiver and fluid temperature distribution along the solar PTC is shown for the single-pass (validated case: case 11, Table 2), $K = 0.55$ double-pass without recycle and $M = 1$ $K = 0.83$ double-pass with recycle with the same boundary conditions. In this figure is shown that the surrounding thermal losses

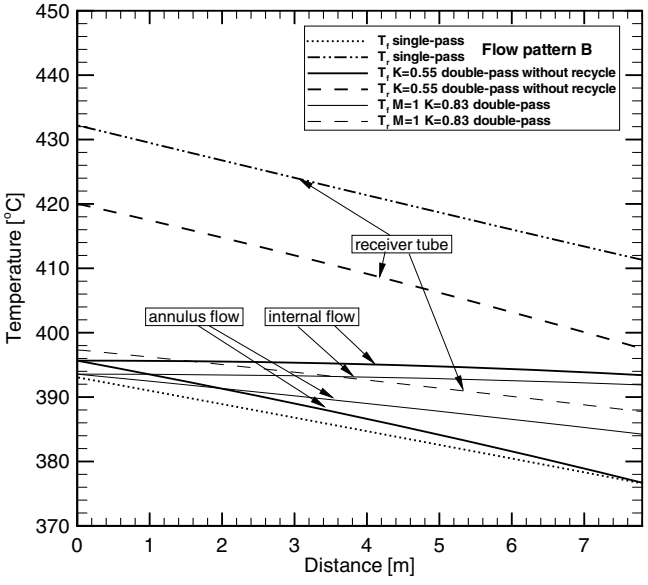

Fig. 8. Fluid and receiver temperature distribution along the solar PTC for three cases with air between receiver and cover: single-pass, flow pattern B $K = 0.55$ double-pass without recycle and flow pattern B $M = 1$ $K = 0.83$ double-pass.

compared with the single-pass device are reduced for the case of $K = 0.55$ double-pass without recycle and $M = 1$ $K = 0.83$ double-pass with recycle due to an important decrement in the receiver temperatures along the solar PTC. This is more evident for the last case ($M = 1$ $K = 0.83$) due to the mass flow rate is higher in the annulus and due to this the quantity of heat absorbed by the fluid is increased significantly compared with the other cases. The improvement of the solar PTC performance for the case of $K = 0.55$ double-pass without recycle and $M = 1$ $K = 0.83$ double-pass with recycle are 1.44 and 3.28%, respectively. However, the friction power expenditure are 10.2 W and 177.24 W, respectively, and for a single-pass is 0.05 W. This additional operating cost and the cost of construct a double-pass device have to be taking into account before take a decision of construct a double-pass solar PTC.

5.3.2. Case of vacuum between receiver and cover (double-pass device)

In these cases, the numerical model considered the convective heat transfer coefficient between the receiver and cover equal to zero.

According to Fig. 9, the desirable effects of increasing heat transfer and reducing surrounding thermal losses increases when the recycle ratio (M), channel thickness ratio (K) and Reynolds number rise. Again as in the case of air between receiver and cover an enhancement of heat transfer rate occurs for flow pattern B with design and operation parameters.

A comparison between the numerical results obtained for air between receiver and cover (case 11, Table 2) and if it will have vacuum between receiver and cover showed that the global thermal efficiency are 56.83% and 63.84%, respectively, or the improvement in the solar PTC performance is 12.4% if vacuum exist between receiver and cover. For the case 7 with vacuum (Table 3) and if it will have air between receiver and cover the improvement obtained is 12.1%. Comparison between air and vacuum in the space between receiver and cover show that global thermal efficiency is significantly degraded by increasing thermal losses when air fills this space.

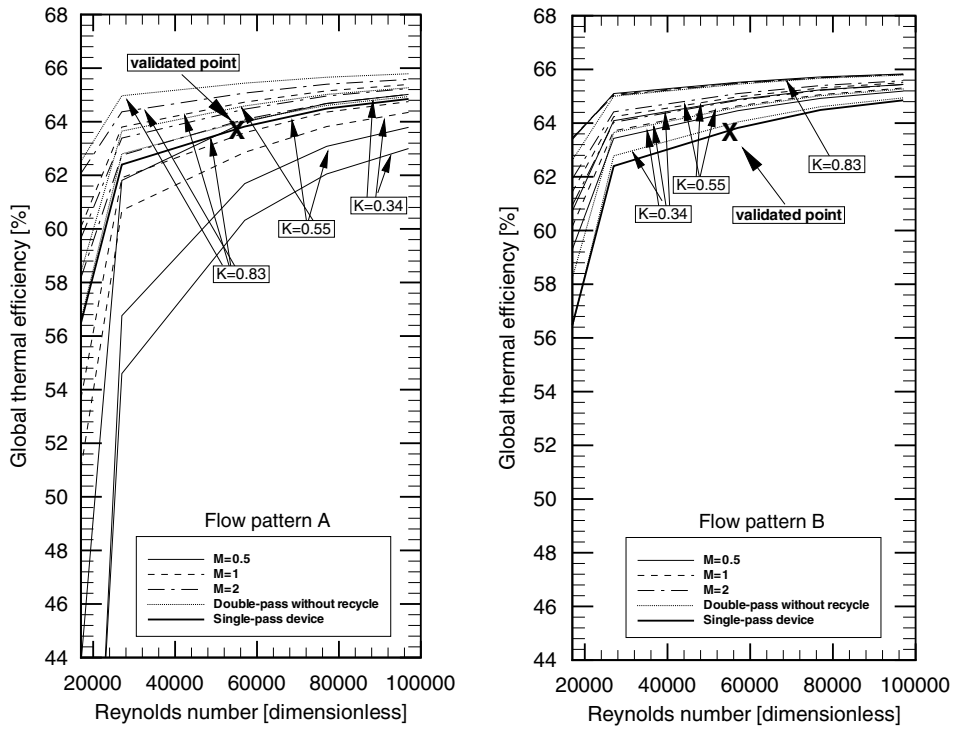

Fig. 9. Global thermal efficiency for a solar PTC with vacuum between receiver and cover vs. *Re* with *K* and *M* as parameters (flow pattern A and B). Validated case (case 9, Table 3).

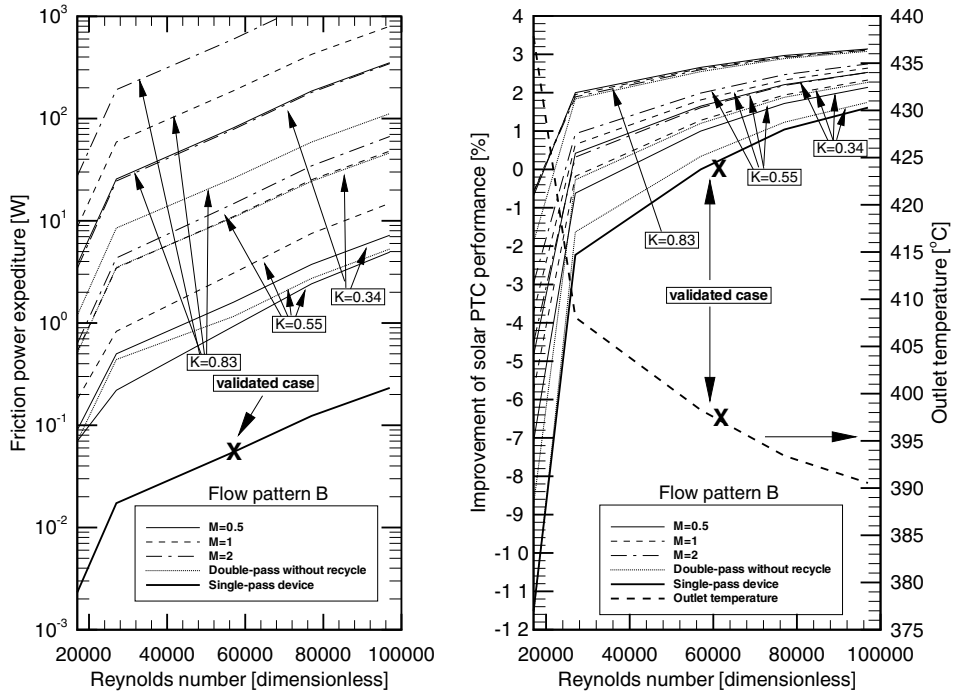

Fig. 10. Friction power expenditure, improvement and outlet temperature for a solar PTC with vacuum between receiver and cover vs. *Re* with *K* and *M* as parameters (flow pattern B). Validated case (case 9, Table 3).

Fig. 10 shows that improvement of solar PTC performance is obtained if the solar PTC is operated with a double-pass device in which the enhancement of convective heat transfer coefficient and consequent in the global thermal efficiency is provided. The advantages are evident with small Reynolds number and diminished when Reynolds number is increased. However for the validated case (case 9, Table 3) the improvement of solar PTC performance with a double-pass device and the same Reynolds number can be of approximately 2.5% and for lower Reynolds number this value can be higher than 10%.

The friction power expenditure increment calculated for the double-pass device is evident in Fig. 10. However, these values

can be still small because the friction power expenditure can be as small as 0.05 W for the validated case (single-pass). The enhancement of heat transfer accompanies increase of hydraulic dissipated energy to maintain the extra friction loss. The evaluation of economical sense including the operating cost in the double-pass heat exchanger is necessary before take a decision to constructing a solar PTC with counter flow concentric circular heat exchangers with or without recycle.

In the same way, the decision between construct a solar PTC with air or vacuum between receiver and cover has to be taken with an economical evaluation of initial and operating cost.

6. Conclusions

A rigorous mathematical model considering the geometrical, optical, thermal and fluid dynamic aspects of a single-pass and double-pass solar PTC has been carried out.

The accuracy of the detailed simulation model is demonstrated in this paper by comparison for increment of temperature, thermal efficiency and thermal losses with steady state experimental data obtained by Sandia National Laboratories for a single-pass solar PTC with air and vacuum in the space between the receiver and cover working with a single-phase water and thermal oil.

Twenty data points evaluated for thermal efficiency in both systems shown a maximum error of 6.02% with a mean deviation of ±2.19%. For the increment of temperature, the maximum error is 5.99% or 1.07 °C with a mean deviation of ±2.25% or ±0.41 °C.

The numerical model is based on the applications of governing equations and used general empirical correlations; for this reason, it is possible to make use of it with greater confidence to other fluids, mixtures and operating conditions (including two-phase flow); it allows using the model developed as an important tool to design and optimize these kinds of systems.

Numerical results shown that improvement in heat transfer is obtained if the solar PTC is operated with external recycle or with a double-pass without recycle. The desirable effects of increasing heat transfer and reducing surrounding thermal losses increases when the recycle ratio, channel thickness ratio and Reynolds number rise. However, the enhancement of heat transfer for double-pass device accompanies increase of hydraulic dissipated energy to maintain the extra friction loss. The evaluation of economical sense including the operating cost in the double-pass heat exchanger is necessary before take a decision to construct a solar PTC with counter flow concentric circular heat exchangers with or without recycle or to decide if vacuum or air technology between receiver and cover is used.

References

[1] S.A. Kalogirou, Solar thermal collectors and applications, Prog. Energy Combust. Sci. 30 (3) (2004) 231–295.
[2] V.E. Dudley, G.J. Kolb, A.R. Mahoney, T.R. Mancini, C.W. Matthews, M. Sloan, D. Kearney, Test results: SEGS LS-2 solar collector, Report of Sandia National Laboratories (SANDIA-94-1884), 1994.
[3] G. Cohen, D. Kearney, Improvement parabolic through solar electric system based on the SEGS experience, in: Proceedings of the ASES Annual Conference, SOLAR 94, 1994, pp. 147–150.
[4] S. Kalogirou, S. Lloyd, J. Ward, Modelling, optimisation and performance evaluation of a parabolic trough solar collector steam generation system, Solar Energy 60 (1) (1997) 49–59.
[5] S.D. Odeh, G.L. Morrison, M. Behnia, Modelling of parabolic through direct steam generation solar collectors, Solar Energy 62 (6) (1998) 395–406.
[6] S.D. Odeh, M. Behnia, G.L. Morrison, Hydrodynamic analysis of direct steam generation solar collectors, J. Solar Energy Eng. 122 (1) (2000) 14–22.
[7] S.D. Odeh, G.L. Morrison, Optimization of parabolic trough solar collector system, Int. J. Energy Res. 30 (4) (2006) 259–271.
[8] J.A. Duffie, W.A. Beckman, Solar Engineering of Thermal Processes, second ed., Wiley Interscience, New York, 1991. pp. 358–361.
[9] F. Kreith, M.S. Bohn, Principles of Heat Transfer, sixth ed., Thomson Learning, 2000.
[10] O. García-Valladares, C.D. Pérez-Segarra, J. Rigola, Numerical simulation of double-pipe condensers and evaporators, Int. J. Refrig. 27 (6) (2004) 656–670.
[11] V. Gnielinski, Equations for heat and mass transfer in turbulent pipe and channel flow, Int. Chem. Eng. 16 (1976) 359–368.
[12] S.W. Churchill, Frictional equation spans all fluid flow regimes, Chem. Eng. 84 (1977) 91–92.
[13] Z. Rouhani, E. Axelsson, Calculation of volume void fraction in the sub-cooled and quality region, Int. J. Heat Mass Transfer 13 (2) (1970) 383–393.
[14] O. Zürcher, J.R. Thome, D. Favrat, Evaporation of ammonia in a smooth horizontal tube: heat transfer measurements and predictions, J. Heat Transfer 121 (1) (1999) 89–101.
[15] F. Friedel, Improved friction pressure drop correlation for horizontal and vertical two-phase pipe flow, in: Proceedings of European Two-Phase Flow Group Meeting, Ispra, Italy, 1979, paper E2.
[16] REFPROP v7.0, Reference fluid thermodynamic and transport properties, NIST Standard Reference Database 23 Gaithersbug, MD 20800, 2002, USA.
[17] http://www.dow.com/heattrans/tech/data.htm.
[18] S.V. Patankar, Numerical Heat Transfer and Fluid Flow, Taylor & Francis, London, 1980. pp. 52–54.
[19] B.V. Karlekar, R.M. Desmond, Engineering Heat Transfer, West Publishing Co., 1977.
[20] S.W. Churchill, H.H.S. Chu, Correlating equations for laminar and turbulent free convection from a horizontal cylinder, Int. J. Heat Mass Transfer 18 (9) (1975) 1049–1053.
[21] C.D. Ho, S.C. Yeh, Improvement in device performance on laminar counterflow concentric circular heat exchangers with uniform wall fluxes, Int. J. Heat Mass Transfer 49 (13–14) (2006) 2020–2032.
[22] M. Jakob, Heat Transfer, John Wiley & Sons, New York, 1949. p. 552.
[23] O. García-Valladares, Numerical simulation of triple concentric-tube heat exchangers, Int. J. Thermal Sci. 43 (10) (2004) 979–991.